



Contents lists available at ScienceDirect

Structures

journal homepage: [www.elsevier.com/locate/structures](http://www.elsevier.com/locate/structures)

# Finite Element Analysis on Mechanical Performance of Middle Long CFST Column with Inner I-Shaped CFRP Profile under Axial Loading

Guochang Li, Ranrui Zhang, Zhijian Yang\*, Bing Zhou

School of Civil Engineering, Shenyang Jianzhu University, Shenyang, China

## ARTICLE INFO

### Article history:

Received 28 January 2016  
Received in revised form 19 August 2016  
Accepted 12 September 2016  
Available online xxx

### Keywords:

Concrete-filled square tube with I-shaped CFRP profile inside  
Middle long column  
Axial load  
Damaged mode  
Mechanical mechanism

## ABSTRACT

The mechanical performance of middle long concrete-filled square steel tube (CFST) column with I-shaped CFRP profile inside was studied in this paper. The numerical model of middle long CFST column with I-shaped CFRP profile inside was established by ABAQUS finite element software on the basis of the reasonable constitutive relationship model of material. The whole process curve of load deformation was analyzed, which can be divided into four stages: elastic stage, elastic-plastic rise stage, elastic-plastic decline stage and rebound stage. The model damaged because of buckling in the mid-span. The effect of steel strength and concrete strength, CFRP profile ratio and thickness of steel tube on mechanical performance of middle long column was studied. The bearing capacity of model increased with the increase of steel strength. With the increase of the concrete strength, the ultimate bearing capacity increased, but the ductility decreased. The ultimate bearing capability increased with the increase the CFRP profile ratio and steel tube thickness.

© 2016 The Institution of Structural Engineers. Published by Elsevier Ltd. All rights reserved.

## 1. Introduction

The concrete-filled steel tube structure (CFT) has the performance of high bearing capacity, convenient construction, good shape and excellent characteristics of fire resistance. The section size of CFT column applied in high-rise buildings was large, the diameter thickness ratio of the tube wall and the confinement coefficient was small. Zhong pointed out that put the materials such as longitudinal and transverse reinforcement steel bar into CFT column could improve the ductility of the structure [1]. The fiber reinforced polymer (FRP) is a kind of excellent-performance material with high strength, anisotropy, corrosion resistance, light weight, low thermal expansion coefficient, good durability and fatigue resistance which is more and more widely used in engineering. Wang and Tao reported the test result of six DSTC models under bending load, which indicated FRP could increase the bearing capacity and stiffness [2]. Wang studied the bearing capacity of DSTC short column under axial compression, and put forward calculation formula [3]. Wang et al. conducted the test of 10 DSTC square columns under axial loading, considering the parameters of hollow rate, cross section of the configuration and CFRP thickness [4]. Nanni reported the test results of AFRP confined concrete under axial compressive and bending load [5]. Mirmiran and Shahawy studied the GFRP confined concrete models subjected to axial loading,

and the result showed that CFRP can effectively restrain the core concrete [6]. Ozbakkaloglu and Akin conducted 24 concrete columns confined by AFRP and CFRP under monotonic and cyclic loading, the results showed that concrete strength and thickness of fiber layer had effect on the model stress-strain curve [7]. Vincent and Ozbakkaloglu conducted the test of 55 high strength and ultra high strength concrete short columns restrained by CFRP, which showed that models had good ductility [8].

Based on the background above, the authors put forward a new kind of concrete-filled square steel tube (CFST) column with I-shaped CFRP profile inside to improve the mechanical property of CFST column. The CFRP is used to bear the vertical load rather than confine the concrete. The I-shaped CFRP profile is putting inside CFST column to increase the bearing capacity and ductility can be, and the weight of the structure will be reduced. Li et al. studied the behavior of CFST short column with I-shaped CFRP profile inside under axial loading [9]. In this paper, model was established by ABAQUS to study the mechanical performance of axial compressed middle long CFST column with I-shaped CFRP profile inside.

## 2. Model design

The section of new type composite column is shown in Fig. 1. The main parameters are the steel strength, thickness of steel tube, concrete strength, slenderness ratio and the section of I-shaped CFRP profile. The details of models are shown in Table 1.

\* Corresponding author.

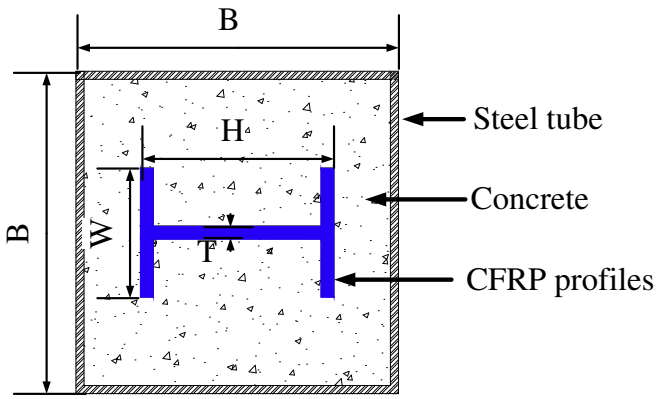


Fig. 1. CFST column with CFRP I-shaped profile inside.

3. Model establishment

3.1. Material constitutive model

3.1.1. Concrete

The concrete strength increases with the increasing of the load as the CFST column with inner I-shaped CFRP profile under axial loading. The stress-strain relationship of concrete is different from unidirectional compressive condition. Considering the applicability of various constitutive relationship for the CFST column with inner I-shaped CFRP profile, the concrete plastic damage model of ABAQUS was used. The concrete constitutive relationship of CFST column proposed by Han et al. [10] was selected, as follows:

$$y = \begin{cases} 2x - x^2 & (x \leq 1) \\ \frac{x}{\beta_0(x-1)^\eta + x} & (x > 1) \end{cases} \quad (1)$$

where,

$$x = \frac{\varepsilon}{\varepsilon_0}; \quad y = \frac{\sigma}{\sigma_0}; \quad \sigma_0 = f_c(N/mm^2); \quad \varepsilon_0 = \varepsilon_c + 800 \cdot \xi^{0.2} \cdot 10^{-6}$$

$$x = \frac{\varepsilon}{\varepsilon_0}; \quad y = \frac{\sigma}{\sigma_0}; \quad \sigma_0 = f_c(N/mm^2); \quad \varepsilon_0 = \varepsilon_c + 800 \cdot \xi^{0.2} \cdot 10^{-6}$$

$$\varepsilon_c = (1300 + 12.5f_c) \cdot 10^{-6}; \quad \xi = \frac{A_s f_y}{A_c f_{ck}}; \quad \eta = 1.6 + 1.5/x; \quad \beta_0 = \frac{f_c^{0.1}}{1.2\sqrt{1+\xi}}$$

$$\varepsilon_c = (1300 + 12.5f_c) \cdot 10^{-6}; \quad \xi = \frac{A_s f_y}{A_c f_{ck}}; \quad \eta = 1.6 + 1.5/x; \quad \beta_0 = \frac{f_c^{0.1}}{1.2\sqrt{1+\xi}}$$

Where  $f_c$  is the cylinder compressive strength of concrete;  $f_{ck}$  is standard value of concrete axial compressive strength;  $f_y$  is the yield strength of steel;  $A_s, A_c$  are the cross section area of steel tube and concrete respectively.

3.1.2. Steel

The simplified ideal elastic-plastic stress-strain relationship of the steel is used, which is shown in Fig. 2.

3.1.3. I-shaped CFRP profile

CFRP profile can be regarded as laminated structure in the simulation, which are mainly carbon fiber unidirectional cloth (Roving) and carbon fiber felt continuous fiber layer (CSM) overlapped. Each layer can be regarded as homogeneous and linear elastic orthogonal anisotropy material [11]. The equivalent thickness is used for each layer, and single layer stiffness performance can be calculated from single fiber volume fraction by mesoscopic mechanics method [12], the strength of a single feature can be determined through standard test method [13]. Failure of I-shaped CFRP profile is based on the secondary development USDFLD subroutine of ABAQUS. Mechanical properties of materials are used in Table 2.

The single-layer failure can be judged by Tsai-Wu failure strength criterion, and limited stiffness degradation of materials can be defined by progressive damage method. Tsai - Wu failure criterion in the state of two-dimensional are as follows [14]:

$$F_{11}\sigma_1^2 + F_{22}\sigma_2^2 + F_{66}\sigma_6^2 + F_1\sigma_1 + F_2\sigma_2 + 2F_{12}\sigma_1\sigma_2 \geq 1 \quad (2)$$

where,

$$F_1 = \frac{1}{X_t} - \frac{1}{X_c}, \quad F_2 = \frac{1}{Y_t} - \frac{1}{Y_c}, \quad F_{11} = \frac{1}{X_t X_c}$$

$$F_{22} = \frac{1}{Y_t Y_c}, \quad F_{12} = -\frac{1}{2\sqrt{X_t X_c Y_t Y_c}}, \quad F_{66} = \frac{1}{S^2}$$

Table 1  
Details of models.

Model	B × t × L/mm	H × W × T/mm	f <sub>y</sub> /MPa	A <sub>s</sub> /mm <sup>2</sup>	f <sub>cu</sub> /MPa	L/B	N <sub>u</sub> /kN
ZC-1	200 × 5 × 1000	120 × 80 × 8	235	2112	40	5	2587.8
ZC-2	200 × 5 × 1000	120 × 80 × 8	345	2112	40	5	3098.2
ZC-3	200 × 5 × 1000	120 × 80 × 8	390	2112	40	5	3288.8
ZC-4	200 × 5 × 1000	120 × 80 × 8	420	2112	40	5	3436.1
ZC-5	200 × 5 × 1800	120 × 80 × 8	420	2112	40	9	3238.2
ZC-6	200 × 5 × 2400	120 × 80 × 8	420	2112	40	12	3113.6
ZC-7	200 × 5 × 1000	120 × 80 × 8	235	2112	30	5	2456.1
ZC-8	200 × 5 × 1000	120 × 80 × 8	235	2112	50	5	2833.3
ZC-9	200 × 5 × 1000	120 × 80 × 8	235	2112	60	5	3241
ZC-10	200 × 5 × 1000	120 × 70 × 6	235	1488	40	5	2372.1
ZC-11	200 × 5 × 1000	140 × 80 × 8	235	2800	40	5	2753.3
ZC-12	200 × 5 × 1000	140 × 80 × 10	235	3200	40	5	3241.5
ZC-13	200 × 4 × 1000	120 × 80 × 8	235	2112	40	5	2358.1
ZC-14	200 × 6 × 1000	120 × 80 × 8	235	2112	40	5	2713.5
ZC-15	200 × 8 × 1000	120 × 80 × 8	235	2112	40	5	3045.2
ZC-16	200 × 5 × 1000	0	235	0	40	5	2199.4

Note: L is the length of the model, f<sub>y</sub> is steel yield strength, A<sub>F</sub> is the cross-sectional area of CFRP, f<sub>cu</sub> is the cubic compressive strength of concrete, N<sub>u</sub> is the ultimate bearing capacity of FEM.

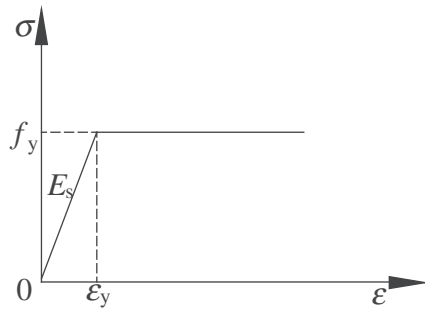


Fig. 2. The stress-strain relationship curve of steel.

Table 2  
Engineering constants of layers in CFRP I-shaped profiles.

Layer	$V_f$	$E_1$ /GPa	$E_2$ /GPa	$\nu_{12}$	$G_{12}$ /GPa	$X_t$ /MPa	$X_c$ /MPa	$Y_t$ /MPa	$Y_c$ /MPa	$S$ /MPa
CSM	0.34	90	80	0.3	4140	700	600	40	120	70
Roving	0.56	120	8.5	0.32	4540	1200	850	50	150	85

Note:  $V_f$  is the fiber volume fraction,  $E_1$  and  $E_2$  are elastic modulus of the fiber direction and vertical direction;  $G_{12}$  is shear modulus,  $\nu_{12}$  is poisson' ratio;  $X_t$ ,  $X_c$  and  $Y_t$ ,  $Y_c$  are the longitudinal and transverse strengths in tension/compression,  $S$  is shear strength.

$$H_1 = F_1\sigma_1 + F_{11}\sigma_1^2, \quad H_2 = F_2\sigma_2 + F_{22}\sigma_2^2, \quad H_6 = F_{66}\sigma_6^2$$

There are three failure modes to be determined according to formula (2): fiber fracture, transverse matrix damage and shear failure inside the facet. The FRP profile has no damage in the initial state. As formula (2) meets the requirements, the material damaged and stiffness degenerated, and  $H_1$  is calculated at the gauss point.

### 3.2. Finite element model

The S4R element was used to simulate the steel tube. The C3D8R element was used to simulate concrete and endplates. S4R composite layer shell element was used to simulate CFRP profile, there are 3

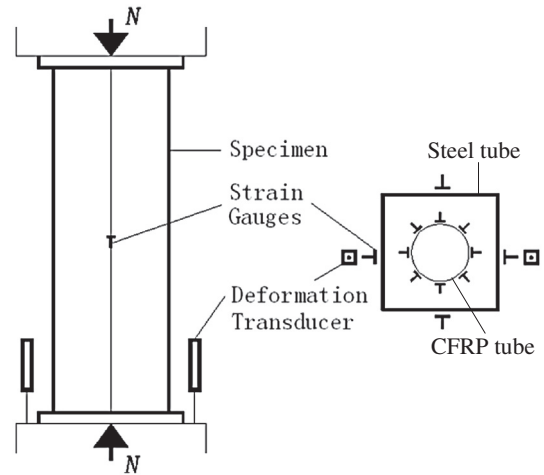


Fig. 4. The test setup of Li et al. [17].

simpson integral points in each layer direction of the shell element. The contact between steel tube and concrete were hard contact, the tangential interaction friction of contact surface was simulated by coulomb friction model of ABAQUS, the friction coefficient is 0.6 referred to Susantha et al. [15] and Hu et al. [16]. CFRP profile and concrete was tied together. The contact between concrete and endplate, steel tube and concrete in the normal direction was hard contact. The contact between steel tube, CFRP profile and endplate was shell- to-solid coupling. Displacement control was used to apply load. The meshes of the finite element models and the boundary conditions are shown in Fig. 3.

### 3.3. Verification of finite element model

The test result of Li et al. [17] was used to verify the FEM model, Fig. 4 is the test setup. Fig.5 shows the typical failure mode of high strength concrete-filled square steel tube columns with inner CFRP circular tube between test and FEM subjected axial loading. It can be seen from Fig. 5 that the failure modes of test and FEM are similar. The experimental axial load-strain curves present by Li et al. [17] are compared

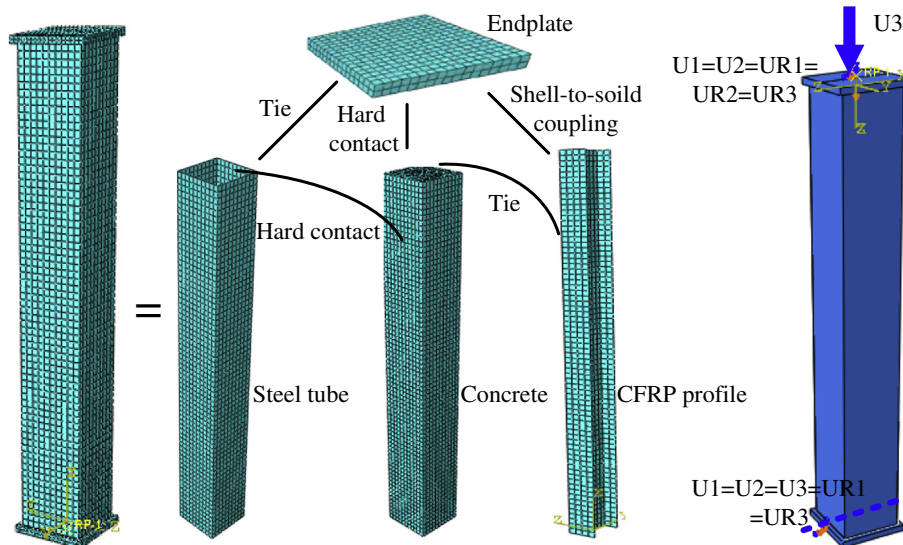


Fig. 3. Assembly and boundary condition of analytical model.

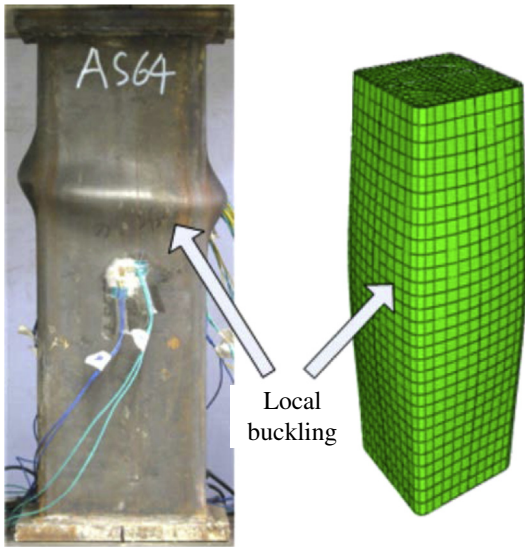


Fig. 5. Comparison of failure mode between test and FEM.

with the FEM results in Fig. 4. The numerical results showed a good agreement with the experimental data (see Fig. 6).

Table 3 shows the full details of the models and the comparisons between the FEM results and the experimental results. Where,  $B$  is cross section height of steel tube;  $t$  is the thickness of steel tube;  $L$  is the length of model;  $\alpha$  is steel ratio;  $\beta$  is carbon fiber ratio, expressed as  $\beta = A_f/A_c$ , where  $A_f$  is CFRP cross-sectional area;  $\xi_s$  is steel confinement factor, expressed as  $\xi_s = \alpha(f_y/f_{ck})$ , where  $f_y$  is yield strength of steel and  $f_{ck}$  is concrete strength.  $\xi_f$  is CFRP confinement factor, expressed as  $\xi_f = \beta(f_f/f_{ck})$ ;  $N_{ue}$  is ultimate bearing capacity of test;  $N_c$  is ultimate bearing capacity of FEM.

The average ratio of  $N_c/N_{ue}$  is 1.02. The data implicated that the finite analysis results coincided with the experimental data, which can accurately simulate experimental results.

#### 4. Results and discussions

##### 4.1. Load-strain curve

The load-displacement curves of ZC-1 and ZC-14 models are shown in Fig. 7. It can be seen from Fig. 7 that there are four stages such as

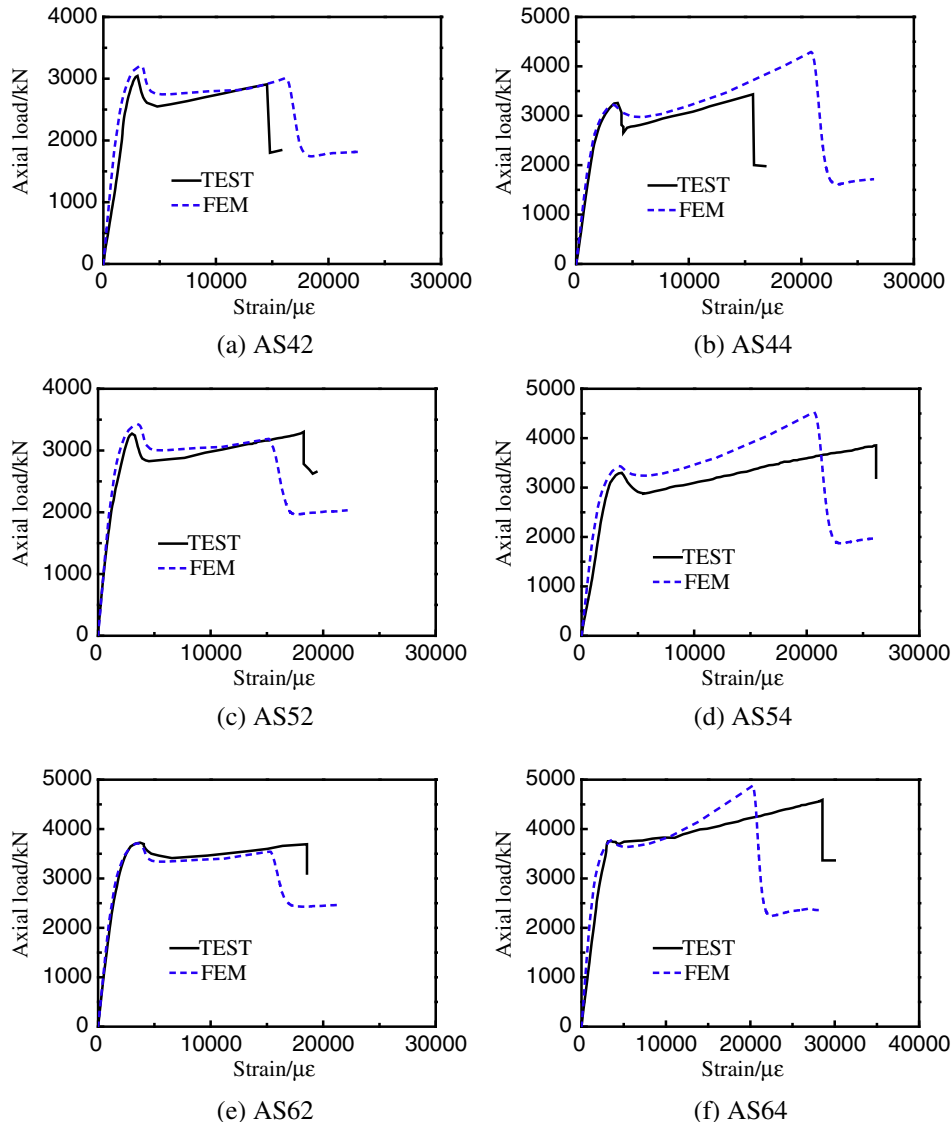


Fig. 6. The axial load versus longitudinal strain Curves of FEM and Test.

**Table 3**  
Test results and calculation results.

Model	B/mm	t/mm	L/mm	$\alpha$	$\beta$	$\xi_s$	$\xi_f$	$N_{ue}/kN$	$N_c/kN$	$N_c/N_{ue}$
AS42	200	4	600	0.0739	0.0107	0.369	0.748	3044	3213	1.06
AS44	200	4	600	0.0739	0.0215	0.369	1.5	3259	3223	0.99
AS52	200	5	600	0.0965	0.0107	0.458	0.748	3274	3430	1.05
AS54	200	5	600	0.0965	0.0215	0.458	1.5	3299	3437	1.04
AS62	200	6	600	0.1269	0.0107	0.689	0.748	3725	3705	0.99
AS64	200	6	600	0.1269	0.0215	0.689	1.5	3755	3769	1.00

elastic stage, elastic-plastic rise stage, elastic-plastic decline stage and rebound stage of middle long CFST column with I-shaped CFRP profile inside. At the beginning of loading, the model was in elastic stage, and concrete, steel tube and CFRP undertook the load together. With the increasing of load, model turned into the elastic-plastic stage, steel tube began to yield, and the concrete cracked, the bearing capacity of the model declined after reaching ultimate bearing capacity. The high performance of the CFRP profile was fully played. The performance of the model degenerated, and entered into the rebound stage, the load-strain curve appeared obviously nonlinear. It is effective to increase the bearing capability and ductility of the model. After putting CFRP profile inside the component, the bearing capability increased by almost 20% compared with CFST.

4.2. Failure mode and working mechanism

At the beginning of loading, the deformation of model was small. As the load reached 60% - 70% of the ultimate bearing capacity, the deformation of mid-span became obvious. When the deformation reached a critical value, the load began to decline, and the deformation increased quickly. As is shown in Fig. 8, the mid-span section of the model damaged outside as drum mode.

Take ZC-1 model as an example to illustrate the ultimate bearing capacity state loading mechanism. The stress distribution of the steel tube, core concrete and CFRP profile are shown in Fig. 9 and Fig. 10.

It can be seen from Fig. 9 and Fig. 10 that the square steel tube had a confinement effect on the core concrete, which made steel tube into bi-axial stress state such as longitudinal stress compression, transverse tensile. The strength of core concrete was significantly higher than the uniaxial compressive strength, large plastic strain appeared at the mid-span. The plastic of zone concrete at CFRP profile web damaged. The stress state of CFRP profile along the height direction was relatively uniform, stress distribution of mid-span was higher, and the outward plastic deformation of mid-span was also large. CFRP profile is a kind of brittle material. Based on the classical laminated plate theory and the end of layer failure strength theory, the stiffness of the layer would decrease as one layer of the laminated material was out of work, so the strength

of CFRP profile would not be invalid. Because of the confinement effect of steel tube, the concrete was in tri-axial compressive stress state, and the bearing capacity of model was improved.

5. Parametric analysis

To further analyze the effects of different parameters, steel yield strength, concrete compressive strength, CRRP profile ratio, steel ratio and slenderness ratio were taken as the variables. The parameters and the corresponding results are shown in Table 1 and Fig. 11.

5.1. Steel yield strength

Fig. 11(a) demonstrates the axial load-deformation curves of the models with different steel yield strength. According to Table 1, the ultimate bearing capacity of model ZC 2, 3 and 4 are 120.1%, 127.5% and 133.2% of the strength of ZC-1. The ultimate bearing capacity of the model increased with the increase of steel tube strength.

5.2. Concrete compressive strength

Fig. 11(b) demonstrates the load-deformation curves of the models with different concrete compressive strength. Fig. 11(b) shows that the ultimate bearing capacity increased with the increase of compressive strength of core concrete, while the ductility reduced. According to Table 1, the ultimate bearing capacity of model ZC-7, 8 and 9 are 94.9%, 109.5% and 125.2% of the strength of ZC-1.

5.3. CRRP profile ratio

Fig. 11(c) demonstrates the load-deformation curves of the models with different CRRP profile ratio  $\rho$  ( $\rho = A_f/A_c$ ,  $A_c$  is the area of concrete).

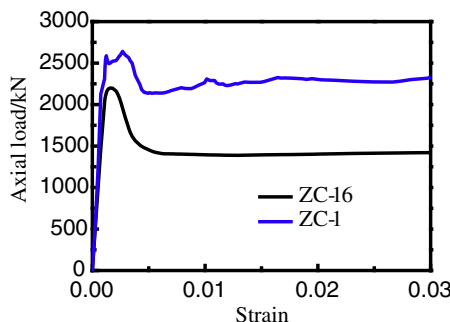


Fig. 7. The impact of CFRP for concrete-filled steel tube long column N-ε curve.

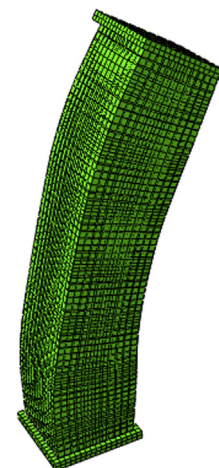


Fig. 8. Failure mode of ZC-1 model.

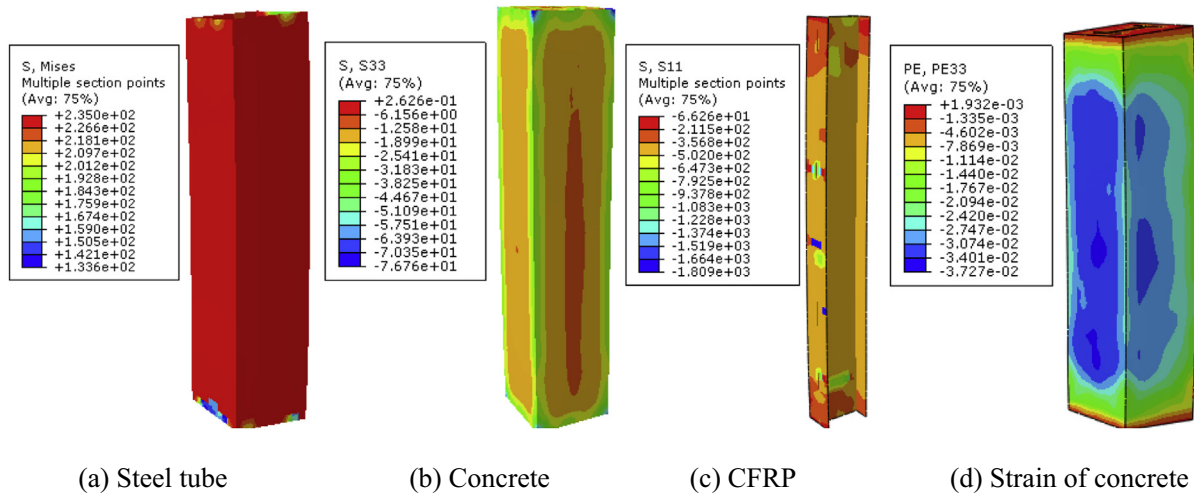


Fig. 9. Stress and strain distribution of ZC-1 model at ultimate state.

According to Table 1, the ultimate bearing capacity of model ZC-10, 11 and 12 are 91.7%, 106.4% and 125.3% of the strength of ZC-1. The ductility enhancement effect is not obvious. The rebound trend is more obvious in the rebound stage following the increase of CRRP profile ratio.

5.4. Steel ratio

Fig. 11(d) demonstrates the load-deformation curves of the models with the different steel ratio. According to Table 1, the ultimate bearing capacity of specimens ZC-13, 14 and 15 are 91.1%, 104.9% and 117.7% of the strength of specimen ZC-1. This is because that the confinement factor increases  $\xi$  with steel ratio, and the concrete ultimate compressive strength also increases with the confinement factor.

5.5. Slenderness ratio

Fig. 11(e) demonstrates the load-deformation curves of the models with the different slenderness ratio. According to Table 1, the ultimate bearing capacity of specimens ZC-5 and 6 are 94.2% and 90.6% of the strength of specimen ZC-4. With the increasing of the slenderness ratio, the ultimate bearing capacity decreases.

6. Conclusions

The conclusion can be reached as follows through ABAQUS nonlinear finite element analysis:

The steel tube, CFRP profile and concrete can work well together. After putting CFRP profile inside, the performance of high strength was fully played, the bearing capacity and ductility performance of models can also be effectively improved.

The mid-span section of middle long CFST column with I-shaped CFRP profile inside damaged outside as drum mode under axial loading.

Parametric analysis showed that the bearing capacity and ductility increased with the increase of steel strength and thickness of steel tube. The bearing capacity increased with the increase of concrete strength, but the ductility slightly reduced. With the increase of CFRP profile ratio, the bearing capacity increased. With the increasing of the slenderness ratio, the ultimate bearing capacity decreases.

Acknowledgements

This project was supported by National Science Foundation of China (5157082947), Innovative Research Team of Higher Education in Liaoning Province (LT2014012), Shenyang Engineering and Technological Research Center for Civil Steel Construction Industrialization (F16-076-8-00).

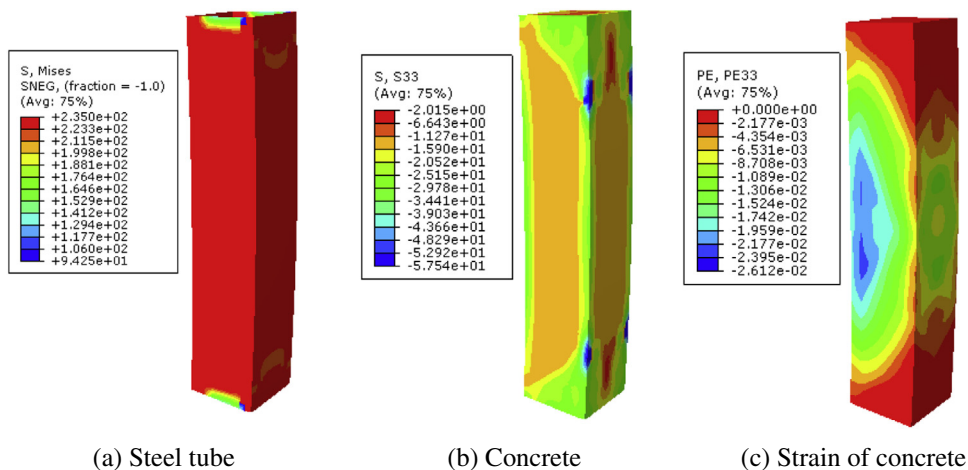


Fig. 10. Stress distribution of ZC-16 model at ultimate state.

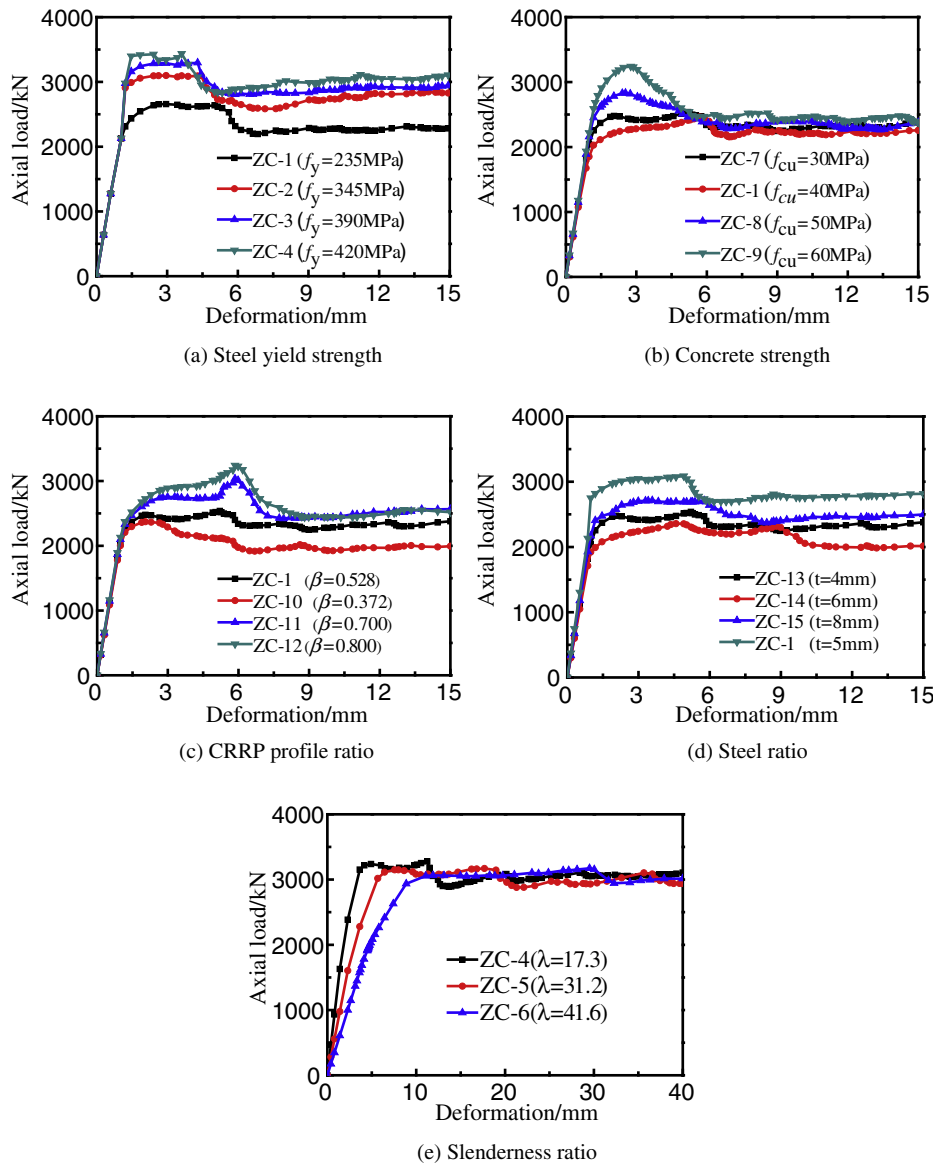


Fig. 11. Comparison of axial load-strain curves.

## References

- [1] Zhong ST. Steel concrete structure. Beijing: Tsinghua University Press; 2003 (in Chinese).
- [2] Wang ZB, Tao Z. Experimental behaviour of FRP-concrete-steel double-skin tubular beams. *Industry Construction* 2009;04:5–8 (in Chinese).
- [3] Wang J, Zhao JH, Zhu Q. Axial bearing capacity of FRP-concrete-steel double-skin tubular short columns. *Industry Construction* 2011;41(11):130–3 (in Chinese).
- [4] Wang D, Wang YZ, Duan XP, Lei QG. Study on axial compression performance of GFRP-concrete-steel tube combined square columns. *Construction Structure* 2014; 15:57–60 (in Chinese).
- [5] Nanni A, Norris MS. FRP jacked concrete under flexure and combined flexure-compression. *Constr Build Mater* 1995;9(5):273–81.
- [6] Mirmiran A, Shahawy M. Behavior of concrete columns confined by fiber composites. *J Struct Eng* 1997;123(5):583–90.
- [7] Ozbakkaloglu T, Akin E. Behavior of FRP-confined normal-and high-strength concrete under cyclic axial compression. *J Compos Constr* 2011;16(4):451–63.
- [8] Vincent T, Ozbakkaloglu T. Influence of concrete strength and confinement method on axial compressive behavior of FRP confined high-and ultra high-strength concrete. *Compos Part B* 2013;50:413–28.
- [9] Li GC, Zhou B, Pan JH. Finite element analysis on concrete-filled square steel tube short columns with inner CFRP profiles under axial compression. *Applied Mechanics and Materials* 2014;578-579:335–9.
- [10] Han LH, Yao GH, Tao Z. Performance of concrete-filled thin-walled steel tubes under pure torsion. *Thin-Walled Struct* 2007;45(1):24–36.
- [11] Davalos JF, Qiao P. A computational approach for analysis and optimal design of FRP beams. *Comput Struct* 1999;70(2):169–83.
- [12] Sonti SS. Stress analysis of pultruded structural shapes. Master thesis Morgantown, West Virginia: West Virginia University; 1992.
- [13] Makkapati S. Compressive strength of pultruded structural shapes. Master thesis Morgantown, West Virginia: West Virginia University; 1994.
- [14] Gol'denblat II, Kopnov VA. Strength of glass-reinforced plastics in the complex stress state. *Polymer Mechanics* 1965;1(2):54–9.
- [15] Susantha KAS, Ge H, Usami T. Confinement evaluation of concrete-filled box-shaped steel columns. *Steel Compos Struct* 2001;1(3):313–28.
- [16] Hu HT, Huang CS, Wu MH, et al. Nonlinear analysis of axially loaded concrete-filled tube columns with confinement effect. *J Struct Eng* 2003;129(10):1322–9.
- [17] Li GC, Lang Y, Yang ZJ. Behavior of high strength CFSST stub columns with inner CFRP tube under axial compressive load. *Adv Steel Constr* 2011;7(3):239–54.